Modelling and Simulation in
Materials Science and Engineering

PURPOSE-LED
PUBLISHING™

You may also like

- Special issue on applied neurodynamics: from neural dynamics to neural engineering
Hillel J Chiel and Peter J Thomas
- Integrability and nonlinear phenomena
David Gómez-Ullate, Sara Lombardo, Manuel Mañas et al.
- Information and Statistical Structure in Spike Trains
Jonathan D Victor and Emery N Brown

A thermodynamic approach to determine accurate potentials for molecular dynamics simulations: thermoelastic response of aluminum

To cite this article: J M Winey *et al* 2009 *Modelling Simul. Mater. Sci. Eng.* **17** 055004

View the article online for updates and enhancements.

This content was downloaded from IP address 88.97.73.214 on 09/10/2024 at 12:12

Modelling Simul. Mater. Sci. Eng. **18** (2010) 029801 (2pp) doi:10.1088/0965-0393/18/2/029801

Corrigendum

Thermodynamic approach to determine accurate potentials for molecular dynamics simulations: thermoelastic response of aluminum

J M Winey, Alison Kubota and Y M Gupta 2009 *Modelling Simul. Mater. Sci. Eng.* **17** 055004

The EAM parameters (table 2) and the effective pair potential (figure 2) do not correspond to the EAM potential that was actually used in the Monte Carlo calculations described in the paper. The correct versions of table 2 and figure 2 are presented here.

Also, equation (16) is incorrect. The correct equation is

$$\begin{aligned} f(r) &= \exp\left[\frac{-(r-b_1)^2}{b_2}\right] && (r < r_m - 1) \\ &= \frac{1}{2}\{1+\cos[\pi(r-r_m+1)]\}\exp\left[\frac{-(r-b_1)^2}{b_2}\right] && (r_m - 1 < r < r_m) \\ &= 0 && (r > r_m), \end{aligned} \tag{16}$$

where the cutoff radius r_m is in angstroms. For $r < 2.25$ Å, spline functions were used in place of equations (15) and (16). The splines were used to provide qualitatively correct $f(r)$ and $\phi(r)$ functions for small r values that were rarely sampled by the Monte Carlo calculations.

In addition, in the caption for figure 4, the last sentence should read 'The solid black curve is the experimental data [8,10].'

Table 2. Parameters for EAM functions (equations (15) and (16)).

Parameter	Fitted value
r_m (Å)	6.365
A (eV Å^{-4})	−1.655 456 076
d_1 (Å^{-1})	−2.192 492 295
d_2 (Å^{-2})	1.998 896 972
d_3 (Å^{-3})	−0.988 327 6548
d_4 (Å^{-4})	0.287 411 7424
d_5 (Å^{-5})	−0.049 315 795 86
d_6 (Å^{-6})	0.004 636 318 247
d_7 (Å^{-7})	−0.000 184 702 4904
b_1 (Å)	2.5
b_2 (Å^2)	0.9

0965-0393/10/029801+02$30.00 © 2010 IOP Publishing Ltd Printed in the UK

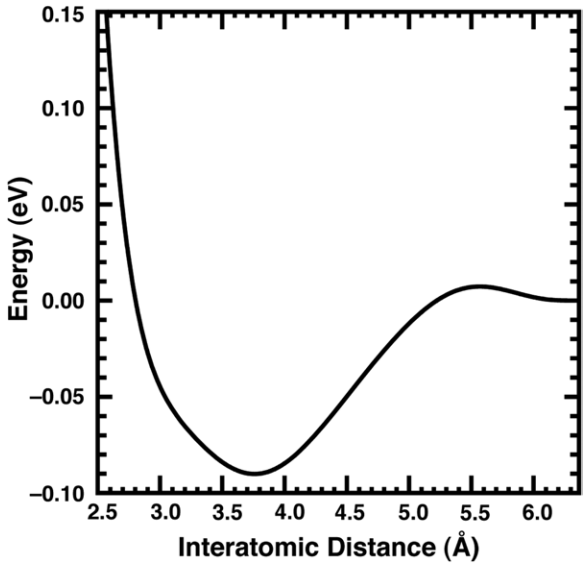

Figure 2. Effective pair potential for aluminum determined using our approach.

Acknowledgment

Dr J A Zimmerman (Sandia National Laboratories, Livermore, CA) is gratefully acknowledged for drawing our attention to the errors in table 2 and equation (16).

Modelling Simul. Mater. Sci. Eng. **17** (2009) 055004 (14pp) doi:10.1088/0965-0393/17/5/055004

A thermodynamic approach to determine accurate potentials for molecular dynamics simulations: thermoelastic response of aluminum

J M Winey[1], **Alison Kubota**[2] **and Y M Gupta**[1]

[1] Institute for Shock Physics and Department of Physics, Washington State University, Pullman, WA 99164, USA
[2] Lawrence Livermore National Laboratory, Livermore, CA 94550, USA

Received 15 October 2008, in final form 5 April 2009
Published 4 June 2009
Online at stacks.iop.org/MSMSE/17/055004

Abstract

An accurate description of the thermoelastic response of solids is central to classical simulations of compression- and deformation-induced condensed matter phenomena. To achieve the correct thermoelastic description in classical simulations, a new approach is presented for determining interatomic potentials. In this two-step approach, values of atomic volume and the second- and third-order elastic constants measured at room temperature are extrapolated to $T = 0\,\mathrm{K}$ using classical thermo-mechanical relations that are thermodynamically consistent. Next, the interatomic potentials are fitted to these $T = 0\,\mathrm{K}$ pseudo-values. This two-step approach avoids the low-temperature quantum regime, providing consistency with the assumptions of classical simulations and enabling the correct thermoelastic response to be recovered in simulations at room temperature and higher. As an example of our approach, an EAM potential was developed for aluminum, providing significantly better agreement with thermoelastic data compared with previous EAM potentials. The approach presented here is quite general and can be used for other potential types as well, the key restriction being the inapplicability of classical atomistic simulations when quantum effects are important.

1. Introduction

In recent years, classical molecular dynamics (MD) simulations have been used increasingly to gain insight into the static and dynamic compression response of solids [1–4]. Results from the MD simulations depend critically on the interatomic potentials, which must accurately represent the actual material systems and be computationally efficient. Because material phenomena such as elastic–plastic deformation and structural phase transitions are governed by the underlying thermoelastic response of the material, a necessary step in establishing the accuracy of a potential, and the resulting validity of the MD simulations, is to evaluate

 © 2009 IOP Publishing Ltd Printed in the UK

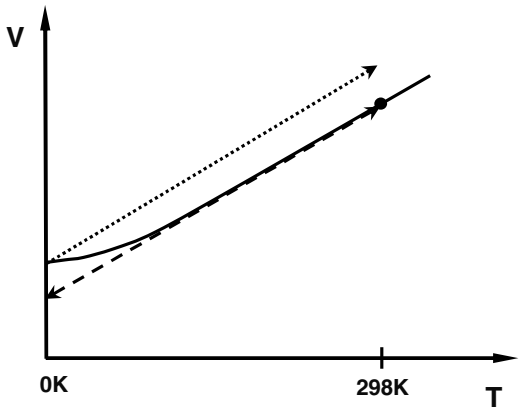

Figure 1. Notional plot of atomic volume versus temperature for solids. The solid curve represents typical experimental data. The dotted line represents typical results from classical simulations (MD or Monte Carlo) performed using potentials fitted to experimental data at low temperatures. The dashed line represents our approach.

predictions of the thermoelastic properties for the thermodynamic conditions of interest. However, such evaluations have not been systematically and consistently incorporated into the development of interatomic potentials. Therefore, substantial discrepancies can exist between the results of classical atomistic simulations and experimental findings.

To enable accurate simulations of the thermoelastic response of materials for the relevant thermodynamic conditions, we have developed a new approach to quantify interatomic potentials. As a test case, this method has been used to determine and evaluate a potential for aluminum single crystals.

The conceptual basis of our approach can be understood by considering a notional plot of atomic volume versus temperature for a typical solid, as shown in figure 1. No significance should be attached to the linearity of the dotted and dashed lines. At low temperatures, the measured volume deviates from the extrapolation of the classical high-temperature behavior due to quantum effects. Because interatomic potentials used in classical MD simulations are typically obtained by fitting low-temperature data and/or results from *ab initio* quantum calculations, classical simulations based on these potentials cannot describe correctly the thermoelastic response at the higher temperatures of interest [5, 6]; note the discrepancy between the dotted and the solid lines in figure 1.

To overcome the problem indicated above, and because our interest is in simulating the material response at room temperature and higher, we avoid the low-temperature quantum regime by using the following approach to determine interatomic potentials. (1) Experimental data obtained at room temperature serve as the starting point of our approach. These data include the atomic volume, second-order elastic constants (SOEC), third-order elastic constants (TOEC) and other available data. (2) The room temperature data are next extrapolated to $T = 0\,\mathrm{K}$ using classical thermo-mechanical relations, as shown notionally in figure 1 for the atomic volume. Thermodynamic consistency is satisfied in this step. (3) The potentials are then fitted to the classically extrapolated $T = 0\,\mathrm{K}$ pseudo-values. (4) Finally, the potentials are tested using classical simulations (MD or Monte Carlo) to verify the recovery of the correct thermoelastic response at room temperature and higher. These steps enable the determination of interatomic potentials using a thermodynamic framework that is consistent with classical atomistic simulations and result in the correct thermoelastic response at the conditions of interest.

The rest of the paper is organized as follows. In the next section, we outline procedures for classically extrapolating representative thermoelastic properties to zero temperature. In section 3, we describe the fitting of an embedded atom method (EAM) potential for aluminum using results from our classical extrapolations. In section 4, we present and discuss results from classical Monte Carlo and MD simulations using our aluminum potential. Our main findings are summarized in section 5.

2. Classical extrapolation of thermoelastic data

The procedure for extrapolating the atomic volume from room temperature to $T = 0\,\mathrm{K}$ is described using isotropic thermodynamics, which is valid for cubic crystals under uniform thermal strains. For noncubic crystals, the approach outlined here can be readily generalized. We write the pressure, for a given atomic volume V, as the sum of an isothermal pressure due to volume compression and a thermal pressure term related to quasiharmonic lattice vibrations. In the quasiharmonic classical limit, $c_V = 3k_\mathrm{B}$ and $(\partial P/\partial T)_V$ is independent of T [7]. Therefore, the pressure is given by

$$P(V,T) = P(V)|_{T=T_\mathrm{ref}} + 3k_\mathrm{B}\,(T - T_\mathrm{ref})\left(\frac{\Gamma}{V}\right), \tag{1}$$

where $P(V)|_{T=T_\mathrm{ref}}$ represents the reference isotherm at $T = T_\mathrm{ref}$ and $\Gamma = V\,(\partial P/\partial E)_V$ is the Gruneisen parameter [8]. Although not required by our method, we simplify this discussion by assuming that Γ/V is constant. Also, because classical atomistic simulations are unable to incorporate contributions from the electronic degrees of freedom, these contributions are neglected in our discussion.

The volume extrapolation is performed by considering a change in temperature from $T_\mathrm{ref} = 298\,\mathrm{K}$ to $T = 0\,\mathrm{K}$ at constant pressure. Therefore, we set $P\,(V_\mathrm{ref}, T_\mathrm{ref}) = P(V,T)$ and use equation (1) to obtain

$$P\,(V_\mathrm{ref})|_{T=T_\mathrm{ref}} = P(V)|_{T=T_\mathrm{ref}} + 3k_\mathrm{B}\,(T - T_\mathrm{ref})\left(\frac{\Gamma}{V}\right). \tag{2}$$

If the reference isotherm is known, then equation (2) can be solved for V at $T = 0\,\mathrm{K}$ to yield the classically extrapolated volume.

The extrapolation of elastic constants to $T = 0\,\mathrm{K}$ requires an anisotropic framework [8]. The temperature change from $T_\mathrm{ref} = 298\,\mathrm{K}$ to $T = 0\,\mathrm{K}$, at constant stress, takes the material from the initial configuration $\bar{x}_i$ to the final configuration x_i via Lagrangian strains η_{ij}. Generalizing equation (1), we define thermodynamic stresses, referenced to the initial configuration $\bar{x}_i$:

$$t_{ij}\,(\eta,\bar{x},T) = \bar{C}^T_{ijkl}\eta_{kl} + \tfrac{1}{2}\bar{C}^T_{ijklmn}\eta_{kl}\eta_{mn} + \tfrac{1}{6}\bar{C}^T_{ijklmnpq}\eta_{kl}\eta_{mn}\eta_{pq} - 3k_\mathrm{B}\,(T - T_\mathrm{ref})\,\Gamma_{ij}/V_\mathrm{ref}, \tag{3}$$

where the $\bar{C}^T$ are isothermal SOEC, TOEC, and fourth-order elastic constants (FOEC) evaluated at the initial configuration $\bar{x}_i$ and the Gruneisen tensor Γ_{ij} [8] is assumed constant, consistent with equation (1). The three strain terms represent a truncated expansion of stress in powers of strain [8, 9].

The second- and third-order elastic coefficients for arbitrary strain are defined as isothermal strain derivatives of the thermodynamic stresses. Therefore,

$$C_{ijkl}\,(\eta,\bar{x},T) = \bar{C}^T_{ijkl} + \bar{C}^T_{ijklmn}\eta_{mn} + \tfrac{1}{2}\bar{C}^T_{ijklmnpq}\eta_{mn}\eta_{pq}, \tag{4}$$

$$C_{ijklmn}\,(\eta,\bar{x},T) = \bar{C}^T_{ijklmn} + \bar{C}^T_{ijklmnpq}\eta_{pq}. \tag{5}$$

These coefficients have no explicit temperature dependence because Γ_{ij} is assumed constant.

The elastic coefficients used in fitting empirical potentials at $T = 0$ K must be referenced to the final configuration, x_i. In general, the transformation from elastic coefficients referenced to configuration $\bar{x}_i$ to those referenced to configuration x_i is given by [8, 9]

$$C_{ijkl}(\eta, x, T) = \frac{V_{\text{ref}}}{V} \frac{\partial x_i}{\partial \bar{x}_m} \frac{\partial x_j}{\partial \bar{x}_n} \frac{\partial x_k}{\partial \bar{x}_p} \frac{\partial x_l}{\partial \bar{x}_q} C_{mnpq}(\eta, \bar{x}, T), \tag{6}$$

$$C_{ijklmn}(\eta, x, T) = \frac{V_{\text{ref}}}{V} \frac{\partial x_i}{\partial \bar{x}_p} \frac{\partial x_j}{\partial \bar{x}_q} \frac{\partial x_k}{\partial \bar{x}_r} \frac{\partial x_l}{\partial \bar{x}_s} \frac{\partial x_m}{\partial \bar{x}_t} \frac{\partial x_n}{\partial \bar{x}_u} C_{pqrstu}(\eta, \bar{x}, T). \tag{7}$$

For thermal expansion of a cubic crystal,

$$\frac{\partial x_1}{\partial \bar{x}_1} = \frac{\partial x_2}{\partial \bar{x}_2} = \frac{\partial x_3}{\partial \bar{x}_3} = \left(\frac{V}{V_{\text{ref}}}\right)^{1/3}. \tag{8}$$

Therefore, equations (6) and (7) become

$$C_{ijkl}(\eta, x, T) = \left(\frac{V}{V_{\text{ref}}}\right)^{1/3} C_{ijkl}(\eta, \bar{x}, T), \tag{9}$$

$$C_{ijklmn}(\eta, x, T) = \left(\frac{V}{V_{\text{ref}}}\right) C_{ijklmn}(\eta, \bar{x}, T). \tag{10}$$

The extrapolation procedures outlined above provide the quantities V, C_{ijkl} and C_{ijklmn}, at $T = 0$ K, to be used for fitting interatomic potentials.

3. Interatomic potential for aluminum

To illustrate the application of our approach, an interatomic potential was determined for aluminum. To enable the fitting of this potential, experimental data for the atomic volume [10], SOEC [11] and TOEC [11] at room temperature were extrapolated to values at $T = 0$ K using the procedures outlined in equations (1)–(10).

To extrapolate the atomic volume, the reference isotherm used in equations (1) and (2) was obtained by fitting the Vinet isotherm [12, 13],

$$P(V) = \frac{3B_0(1 - X)}{X^2} \exp\left[\frac{3}{2}\left(B' - 1\right)(1 - X)\right], \tag{11}$$

$$X = \left(\frac{V}{V_{\text{ref}}}\right)^{1/3}, \tag{12}$$

to hydrostatic compression data for aluminum at room temperature [14, 15]. In equation (11), B_0 is the isothermal bulk modulus at zero pressure and B' is its pressure derivative. Using this isotherm, the volume at $T = 0$ K was determined using equation (2) and the resulting value is shown in column 1 of table 1. Also, the extrapolated P–V isotherm at $T = 0$ K was obtained using equation (1), with the resulting B_0 and B' parameters listed in column 1 of table 1.

To extrapolate the elastic constants, the measured isentropic SOEC [11] and thermodynamically mixed TOEC [11] were first converted to isothermal constants as described in appendix A. To maintain consistency with hydrostatic compression data [14, 15], the TOEC were adjusted slightly (within the experimental uncertainty bounds [11]) as described in appendix B. The hydrostatic compression data were also used to estimate the isothermal FOEC, using the approximations proposed in [16] (see appendix C). Finally, the classical

Table 1. Extrapolated values at $T = 0$ K used in fitting the aluminum EAM potential and calculated values at $T = 0$ K using the fitted potential. The values shown are the atomic volume (V), SOEC (C_{ij}) and TOEC (C_{ijk}) for Al, where the SOEC and TOEC are expressed in the abbreviated Voigt notation [36]. Also shown are the isothermal bulk modulus (B_0) and pressure derivative (B') from the Vinet isotherm, the vacancy formation energy (E_V), the stacking fault energy (E_{SF}) and the phonon frequencies at the X-point in the Brillouin zone (ν_L and ν_T).

	Extrapolated values (except as noted)	Calculated values
V (Å^3)	16.31[a]	16.31
C_{11} (GPa)	114.7[b]	113.7
C_{12} (GPa)	61.24[b]	61.7
C_{44} (GPa)	32.86[b]	31.2
C_{111} (GPa)	−1130[b]	−1187
C_{112} (GPa)	−348[b]	−351
C_{123} (GPa)	+28[b]	+53
C_{144} (GPa)	−19[b]	−6.5
C_{166} (GPa)	−362[b]	−358
C_{456} (GPa)	−29[b]	−30
B_0 (GPa)	79.06[c]	79.07
B' (unitless)	4.487[c]	4.478
E_V (eV)	0.66[d]	0.63
E_{SF} (mJ m^{-2})	145[e]	142
ν_L (THz)	9.69[f]	9.90
ν_T (THz)	5.80[f]	6.10

[a] Classically extrapolated to $T = 0$ K using data from [10].
[b] Classically extrapolated to $T = 0$ K using data from [11].
[c] Classically extrapolated to $T = 0$ K using data from [14, 15].
[d] $T = 298$ K value [19].
[e] $T = 298$ K value [20, 21].
[f] $T = 80$ K value [22].

extrapolations to $T = 0$ K were performed using the procedures outlined in equations (3)–(10). The resulting values at $T = 0$ K for the SEOC and TOEC of aluminum are shown in the first column of table 1.

To incorporate the TOEC, we utilized the method of Chantasiriwan and Milstein (CM) [17] for the determination of an EAM potential. We emphasize that, while EAM potentials are convenient for our approach, the extrapolation methods outlined in equations (1)–(10) are general and can be applied to other potential types as well.

In the EAM approach [18], the energy is written as the sum of two components—a pairwise interaction term and an embedding term that incorporates many-body interactions:

$$E = \sum_{i \neq j} \phi\left(r_{ij}\right) + F\left(\bar{\rho}\right), \tag{13}$$

$$\bar{\rho} = \sum_{i \neq j} f\left(r_{ij}\right), \tag{14}$$

where $\phi(r_{ij})$ is the pairwise potential, $F(\bar{\rho})$ is the embedding energy for an atom in a host electron density $\bar{\rho}$ and the summations are over pairs of atoms. In [17], CM related combinations of SOEC and TOEC to derivatives of $\phi(r_{ij})$ and $f(r_{ij})$, providing constraints that were used in determining $\phi(r_{ij})$ and $f(r_{ij})$ from the experimental data. The embedding energy $F(\bar{\rho})$ was obtained from equation (13), with $E(V)$ determined from a fit to hydrostatic compression data.

Table 2. Parameters for EAM functions (equations (15) and (16)).

Parameter	Fitted Value
r_m (Å)	6.365
A (eV Å^{-4})	−3.0512
d_1 (Å^{-1})	−2.0305
d_2 (Å^{-2})	1.7369
d_3 (Å^{-3})	−0.812 98
d_4 (Å^{-4})	0.225 26
d_5 (Å^{-5})	−0.037 011
d_6 (Å^{-6})	0.003 3455
d_7 (Å^{-7})	−0.000 128 59
b_1 (Å)	2.5
b_2 (Å^2)	0.9

To determine an EAM potential for aluminum, the $T = 0$ K values (column 1 of table 1) extrapolated from room temperature data were used to fit the following EAM functions [17]:

$$\phi(r) = A(r - r_m)^4 \left(1 + d_1 r + d_2 r^2 + d_3 r^3 + d_4 r^4 + d_5 r^5 + d_6 r^6 + d_7 r^7\right), \tag{15}$$

$$f(r) = \exp\left[\frac{-(r - b_1)^2}{b_2}\right], \tag{16}$$

where r_m is the cutoff radius. Our use of a Gaussian function in equation (16) differs from the $f(r)$ used in [17]. To determine $F(\bar{\rho})$ using equation (13), $E(V)$ was fitted to the extrapolated P–V isotherm at $T = 0$ K (see B_0 and B' in table 1). While not included in the formal fitting process, the cutoff radius r_m shown in table 2 provided a good match between simulated and experimental results at high temperatures.

In addition to the extrapolated values of the elastic constants and the 0 K isotherm, other data used to constrain our EAM potential included the vacancy formation energy [19], the stable stacking fault energy [20, 21] and the $T = 80$ K phonon frequencies at the X-point in the Brillouin zone [22]. These defect energies and phonon frequencies were not extrapolated to $T = 0$ K because the information required for the extrapolation was not available.

The aluminum potential determined using the methods described here is shown in figure 2 in the effective pair format. Parameter values determined for the functions in equations (15) and (16) are listed in table 2. To indicate the quality of the fit to the values in column 1 of table 1, values calculated using the Al potential are listed in column 2 of table 1. Overall, the two sets of values match well.

4. Results of aluminum simulations

To perform an initial test of our potential for aluminum, we calculated the phonon frequencies at zero temperature. As shown in figure 3, our calculated phonon dispersion curves show good agreement with the experimental data (obtained at $T = 80$ K) [22].

As a more stringent test, we used our potential to determine the thermoelastic response at finite temperatures using the method of strain fluctuations [23] in the Metropolis Monte Carlo [24] framework. For any single simulation, a system of 500 atoms with an initially perfect fcc configuration was equilibrated for one million Monte Carlo iterations, followed by a production run of nine million iterations. From these calculations, we extracted thermoelastic

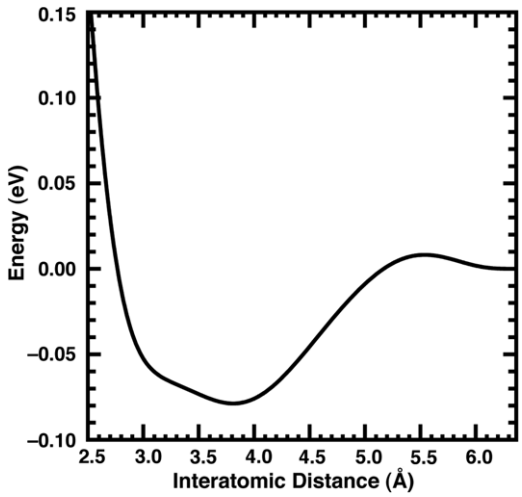

Figure 2. Effective pair potential for aluminum determined using our approach.

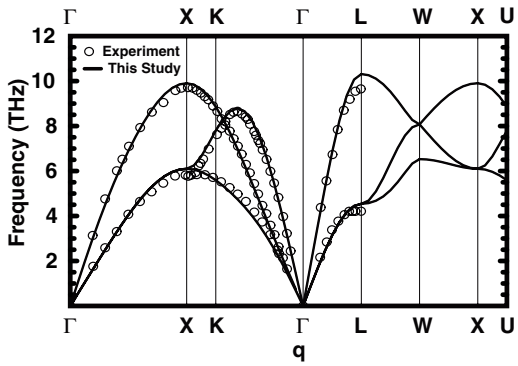

Figure 3. Phonon dispersion curves for aluminum. The circles are experimental data obtained at $T = 80\,\mathrm{K}$ [22]. The solid lines are calculations using our potential.

properties such as atomic volume, isentropic SOEC, thermal expansion coefficient and specific heat. Simulations to obtain these properties were performed over a range of temperatures.

In figure 4, we show calculated atomic volumes using our potential, and compare them with experimental data [10] and with calculated volumes using several previous EAM potentials: CM [25], Ercolessi and Adams (EA) [26] and Mishin *et al* (MFMP) [27]. These plots show that our potential, which was fitted to the classically extrapolated volume at $T = 0\,\mathrm{K}$, is able to provide a very good description of the atomic volumes at higher temperatures. In contrast, the CM and EA potentials were fitted to the experimentally measured volume at low temperature. Therefore, because the measured low-temperature volume deviates from the extrapolation of the classical high-temperature behavior due to quantum effects, the CM and EA potentials are unable to recover the correct higher-temperature response in classical simulations. The performance of the MFMP potential is worse than the others because it was fitted to the experimental volume at room temperature. The results in figure 4 demonstrate the effectiveness of our extrapolation method for fitting interatomic potentials.

Next, the specific heat at constant pressure (c_P) is considered in figure 5, where calculated results using our potential are compared with experimental data [28, 29] and with results

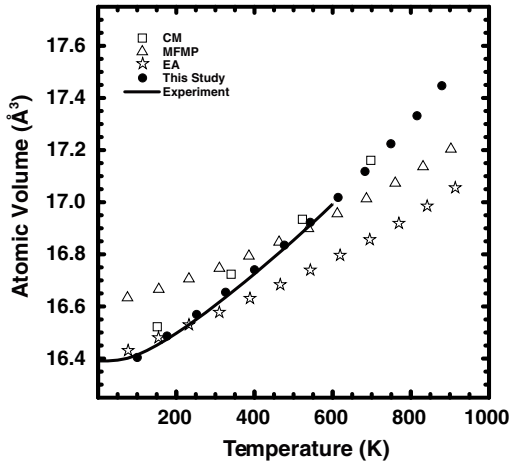

Figure 4. Atomic volume versus temperature for aluminum. The symbols indicate calculations using our potential—filled circles; the CM potential [25]—open squares; the MFMP potential [27]—open triangles and the EA potential [26]—open stars. The solid black curve is the experimental data [10].

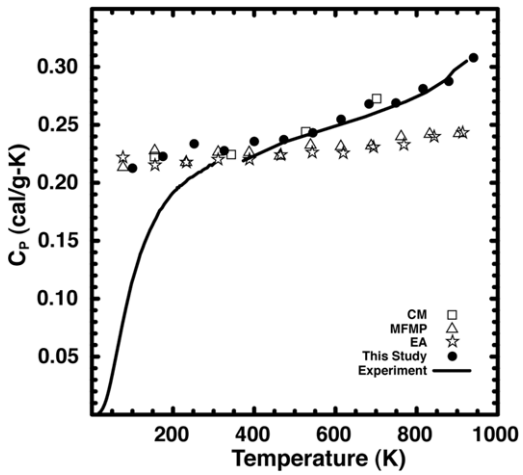

Figure 5. Specific heat at constant pressure versus temperature for aluminum. The symbols indicate calculations using our potential—filled circles; the CM potential [25]—open squares; the MFMP potential [27]—open triangles and the EA potential [26]—open stars. The solid black curves are the experimental data [28, 29].

using the previous potentials [25–27]. At low temperatures, where quantum effects dominate, classical simulations cannot provide a correct description of the specific heat, as expected. At higher temperatures, where classical thermodynamics is valid, our potential provides better agreement with the experimental data compared to results using the EA and MFMP potentials, whereas the calculated c_P values obtained using the CM potential are similar to those obtained using our potential. The failure of the EA and MFMP potentials to describe the high temperature behavior of c_P is related in part to their poor description of thermal expansion, shown in figure 4.

The temperature dependence of the isentropic SOEC is shown in figure 6. Calculated results using our potential agree more closely with the experimental data [30, 31], compared with the previous potentials [25–27]. The contrast is particularly noteworthy for C_{11}, where the

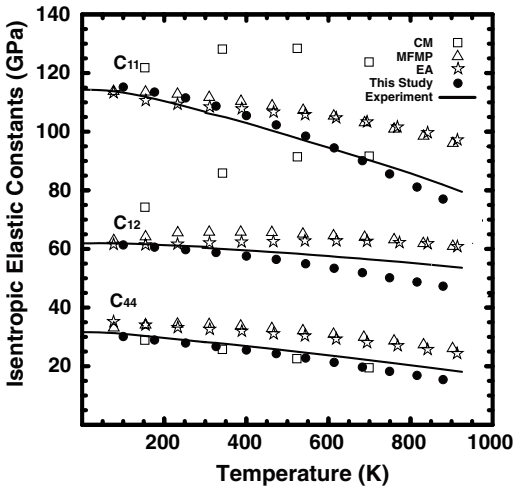

Figure 6. Second-order elastic constants versus temperature for aluminum. The symbols indicate calculations using our potential—filled circles; the CM potential [25]—open squares; the MFMP potential [27]—open triangles and the EA potential [26]—open stars. The solid black curves are the experimental data [30, 31].

previous potentials do not provide sufficient softening at high temperature. The temperature dependence of the SOEC depends strongly on both the TOEC and the thermal expansion coefficient. Therefore, the better description obtained using our potential provides further validation for our classical extrapolation method and illustrates the importance of including anharmonic lattice properties, such as the TOEC, in the data set for fitting interatomic potentials. Although the CM potential [25] incorporates information from the TOEC, figure 6 shows that the SOEC determined using this potential display unphysical behavior; the temperature derivatives for C_{11} and C_{12} have the wrong sign at moderate temperatures. Further work is needed to determine the reason for this behavior of the CM potential.

Calculated values for the Grüneisen parameter (Γ) are shown in figure 7. These values are compared with experimental values obtained from a direct measurement [32] at room temperature, and from an indirect determination that used thermo-mechanical data [10, 29, 31] in the thermodynamic relation [8]

$$\Gamma = \frac{V\beta\,(C_{11} + 2C_{12})}{3c_P}, \tag{17}$$

where β is the volume thermal expansion coefficient. As shown in the figure, calculated results using our potential agree much better with the experimental data, compared with results using the previous potentials [25–27]. An accurate determination of the Grüneisen parameter is of particular importance for dynamic compression simulations because the magnitude of the thermal stress contribution is strongly dependent on Γ (see equations (1) and (3)).

Finally, the melting temperature for aluminum at ambient pressure was calculated using an MD approach described previously [33]. Using our potential, we obtained a melting temperature of 840 K $\pm$ 20 K, compared with the experimental value of 933 K [34]. Melting temperatures for other EAM potentials include 939 K (EA) [26], 1027 K (MFMP) [35] and 800 K $\pm$ 30 K (CM). The accuracy of our results compares well with the accuracy obtained using the MFMP and CM potentials, but is not as good as that reported in [26].

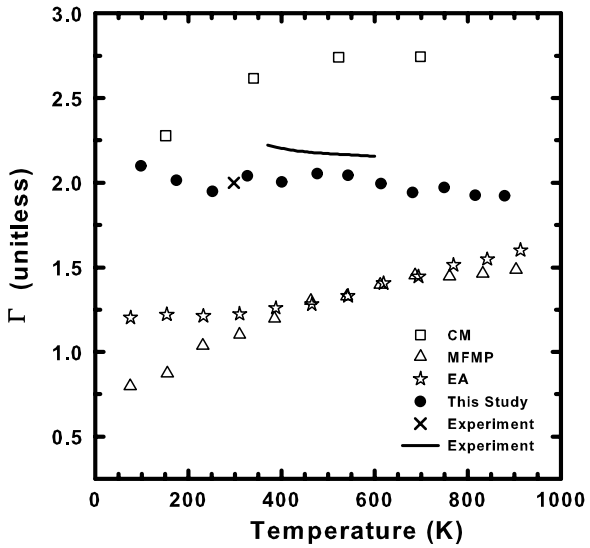

Figure 7. Grüneisen parameter versus temperature for aluminum. The symbols indicate calculations using our potential—filled circles; the CM potential [25]—open squares; the MFMP potential [27]—open triangles and the EA potential [26]—open stars. The symbol **x** denotes the result of a direct measurement at room temperature [32]. The solid black curve results from an indirect determination using thermo-mechanical data [10, 29, 31] in equation (17).

5. Summary and conclusions

A new approach for determining interatomic potentials for classical MD simulations was developed. This development was motivated by the objective to ensure the correct thermoelastic response in classical simulations of compression- and deformation-induced condensed matter phenomena. In our approach, a thermodynamically consistent framework is used to extrapolate experimentally measured thermo-mechanical results at room temperature to pseudo-values at $T = 0$ K. Because our extrapolation approach is purely classical, it avoids the low-temperature quantum regime. The term pseudo-values is used to distinguish our extrapolated values from the actual physical values at $T = 0$ K. The pseudo-values are then used to obtain the interatomic potentials. These potentials, in turn, ensure the correct thermoelastic response in classical simulations at room temperature and higher temperatures.

As an example of this approach, an EAM potential was developed for aluminum single crystals. Classical simulation results, using this potential, provided significantly better agreement with experimental data at higher temperatures, compared with previous EAM potentials. Although the proposed framework is particularly convenient for EAM potentials, the classical extrapolation procedure is general and is applicable to other potential types as well. Because our entire development is classical, it is inapplicable when quantum effects are important.

Acknowledgments

Dr M Asta is thanked for useful discussions regarding the calculation of melting temperatures. Dr M Desjarlais is acknowledged for suggesting the Grüneisen parameter calculations. Computer resources were provided by Livermore Computing at Lawrence Livermore National

Laboratory. This work was supported by the US Department of Energy under Grant DE-FG03-97SF21388 (Washington State University) and Contract W-7405-Eng-48 (Lawrence Livermore National Laboratory).

Appendix A

The measured isentropic SOEC [11] were converted to isothermal values using the thermodynamic relation [8]

$$C^S_{ijkl} - C^T_{ijkl} = \frac{c_\eta T \Gamma_{ij} \Gamma_{kl}}{V_{\text{ref}}}, \tag{A1}$$

where c_η is the specific heat at constant strain. For the TOEC, the experimental values were obtained by measuring changes in the isentropic sound speeds due to an applied isothermal strain [11]. Therefore, the measured TOEC are thermodynamically mixed, denoted by the symbol C^{SST}_{ijklmn}. To convert the mixed coefficients to fully isothermal values, we took the isothermal strain derivative of (A1) to obtain

$$C^{SST}_{ijklmn} - C^T_{ijklmn} = \frac{c_\eta T}{V_{\text{ref}}} \frac{\partial}{\partial \eta_{mn}} \left[\Gamma_{ij} \Gamma_{kl}\right]_T . \tag{A2}$$

Therefore, under the thermodynamic assumptions that we have made for our thermodynamic extrapolations ($c_\eta = 3k_B$, Γ_{ij} constant), the measured mixed TOEC and the isothermal TOEC are equivalent.

Appendix B

To examine the consistency of the measured elastic constants [11] with the isothermal P–V data [14, 15], we performed a term-by-term comparison of the strain expansion for the Cauchy stresses under hydrostatic loading with the strain expansion for the Vinet P–V isotherm. The measured Cauchy stresses are referenced to the current configuration, x, and are related to the thermodynamic stresses defined in equation (3) [9]:

$$\sigma_{rs}(\eta, x, T) = \frac{V_{\text{ref}}}{V} \frac{\partial x_r}{\partial \bar{x}_i} \frac{\partial x_s}{\partial \bar{x}_j} t_{ij}(\eta, \bar{x}, T) . \tag{B1}$$

Here we consider $T = T_{\text{ref}} = 298$ K, so that the thermal contribution to the stresses is zero. For hydrostatic loading of a cubic crystal, equation (8) is applicable. Therefore, the Lagrangian strains are given by [9]

$$\eta_{11} = \eta_{22} = \eta_{33} = \frac{1}{2}\left[\left(\frac{V}{V_{\text{ref}}}\right)^{2/3} - 1\right]. \tag{B2}$$

Using (3), (8) and (B2), we expand equation (B1) in powers of strain to obtain

$$\begin{aligned}\sigma_1 = \sigma_2 = \sigma_3 = {} & \left(\bar{C}^T_{11} + 2\bar{C}^T_{12}\right)\eta_1 + \left[-\left(\bar{C}^T_{11} + 2\bar{C}^T_{12}\right) + \frac{1}{2}\left(\bar{C}^T_{111} + 6\bar{C}^T_{112} + 2\bar{C}^T_{123}\right)\right]\eta_1^2 \\ & + \left[\frac{3}{2}\left(\bar{C}^T_{11} + 2\bar{C}^T_{12}\right) - \frac{1}{2}\left(\bar{C}^T_{111} + 6\bar{C}^T_{112} + 2\bar{C}^T_{123}\right)\right. \\ & \left. + \frac{1}{6}\left(\bar{C}^T_{1111} + 8\bar{C}^T_{1112} + 6\bar{C}^T_{1122} + 12\bar{C}^T_{1123}\right)\right]\eta_1^3,\end{aligned} \tag{B3}$$

where the contracted Voigt notation [36] for the tensor indices has been used.

To expand the Vinet isotherm [12, 13] in powers of the Lagrangian strain, we solve equation (B2) for $(V/V_{\mathrm{ref}})^{1/3}$ and substitute into equation (11). Expanding (11) in a Taylor series to third order in strain, we obtain

$$-P(V) = 3B_0\eta_1 - 3B_0\left(1+\frac{3B'}{2}\right)\eta_1^2 + 3B_0\left(\frac{17}{8}+\frac{9B'}{4}+\frac{9B'^2}{8}\right)\eta_1^3, \tag{B4}$$

where the negative of the pressure has been used to enable a direct comparison with equation (B3). Equating (B4) to (B3) term by term, we obtain the desired consistency relations:

$$3B_0 = \left(\bar{C}_{11}^T + 2\bar{C}_{12}^T\right), \tag{B5}$$

$$-3B_0\left(1+\frac{3B'}{2}\right) = -\left(\bar{C}_{11}^T + 2\bar{C}_{12}^T\right) + \frac{1}{2}\left(\bar{C}_{111}^T + 6\bar{C}_{112}^T + 2\bar{C}_{123}^T\right), \tag{B6}$$

$$\begin{aligned} 3B_0\left(\frac{17}{8}+\frac{9B'}{4}+\frac{9B'^2}{8}\right) &= \frac{3}{2}\left(\bar{C}_{11}^T + 2\bar{C}_{12}^T\right) - \frac{1}{2}\left(\bar{C}_{111}^T + 6\bar{C}_{112}^T + 2\bar{C}_{123}^T\right) \\ &\quad + \frac{1}{6}\left(\bar{C}_{1111}^T + 8\bar{C}_{1112}^T + 6\bar{C}_{1122}^T + 12\bar{C}_{1123}^T\right), \end{aligned} \tag{B7}$$

To apply these relations, we begin by evaluating (B5) using the isothermal elastic constants at $T = 298\,\mathrm{K}$, which were determined from the measured isentropic values [11] using equation (A1) and $\Gamma_{11} = \Gamma_{22} = \Gamma_{33} = 2.01$ [32]; the result is

$$B_0 = 72.85\,\mathrm{GPa}. \tag{B8}$$

Keeping B_0 fixed, we fit the Vinet isotherm to the hydrostatic compression data [14, 15] to obtain

$$B' = 4.561. \tag{B9}$$

Substituting into (B6), we find that (B9) is not consistent with the measured TOEC [11]. To enforce consistency, the TOEC were re-determined from the data [11] using a weighted least squares analysis where equations (B6), (B8) and (B9) were incorporated as additional constraints. The resulting set of TOEC at $T = 298\,\mathrm{K}$ is

$$\begin{aligned} C_{111} &= -1093.9\,\mathrm{GPa}, \\ C_{112} &= -325.4\,\mathrm{GPa}, \\ C_{123} &= +28.1\,\mathrm{GPa}, \\ C_{144} &= -19.8\,\mathrm{GPa}, \\ C_{155} &= -339.8\,\mathrm{GPa}, \\ C_{456} &= -30\,\mathrm{GPa}. \end{aligned} \tag{B10}$$

The differences between these values and the reported TOEC [11] are within the reported experimental uncertainties.

Appendix C

Based on the idea that pairwise repulsive forces are dominant in determining the higher order elastic constants for noble metals, Hiki and Granato [16] suggested the following approximate relationships for the TOEC:

$$\begin{aligned} C_{111} &= 2C_{112} = 2C_{155}; \\ C_{123} &= C_{144} = C_{456} = 0. \end{aligned} \tag{C1}$$

For aluminum, these relations are in qualitative agreement with the TOEC values given in (B10). Using similar arguments, Hiki and Granato suggested approximate relationships for the FOEC:

$$C_{1111} = 2C_{1112} = 2C_{1122} = 2C_{1155} = 2C_{1266} = 2C_{4444};$$
$$C_{1123} = C_{1144} = C_{1244} = C_{1456} = C_{4455} = 0. \tag{C2}$$

Under these assumptions, the full set of fourth-order constants is determined from C_{1111} alone. Therefore, to provide an estimated set of FOEC for aluminum, the relations in (C2) were employed and C_{1111} was determined from hydrostatic compression data [14, 15]. Inserting (C2) into (B7), we obtain

$$3B_0\left(\frac{17}{8} + \frac{9B'}{4} + \frac{9B'^2}{8}\right) = \frac{3}{2}(C_{11} + 2C_{12}) - \frac{1}{2}(C_{111} + 6C_{112} + 2C_{123}) + \frac{4}{3}C_{1111}. \tag{C3}$$

Using the results from equations (B8)–(B10), equation (C3) was solved for C_{1111} at $T = 298$ K to obtain

$$C_{1111} = 4500\,\text{GPa}. \tag{C4}$$

The remaining fourth-order constants were then determined using (C2):

$$C_{1112} = C_{1122} = C_{1155} = C_{1266} = C_{4444} = 2250\,\text{GPa},$$
$$C_{1123} = C_{1144} = C_{1244} = C_{1456} = C_{4455} = 0. \tag{C5}$$

The accuracy of these approximations is adequate for our purposes because the FOEC are used only in the thermodynamic extrapolation of the SOEC and TOEC to $T = 0$ K.

References

[1] Belonoshko A B, Ahuja R and Johansson B 2003 *Nature* **424** 1032
[2] Holian B L and Lomdahl P S 1998 *Science* **280** 2085
[3] Kadau K, Germann T C, Lomdahl P S and Holian B L 2002 *Science* **296** 1681
[4] Bringa E M, Rosolankova K, Rudd R E, Remington B A, Wark J S, Duchaineau M, Kalantar D H, Hawreliak J and Belak J 2006 *Nature Mater.* **5** 805
[5] Swanson R E, Straub G K, Holian B L and Wallace D C 1982 *Phys. Rev.* B **25** 7807
[6] Wallace D C 2002 *Statistical Physics of Crystals and Liquids* (New Jersey: World Scientific) p 198
[7] Born M and Huang K 1954 *Dynamical Theory of Crystal Lattices* (New York: Oxford)
[8] Wallace D C 1972 *Thermodynamics of Crystals* (New York: Wiley)
[9] Wallace D C 1970 *Solid State Physics* vol 25 ed H Ehrenreich *et al* (New York: Academic) p 301
[10] Cooper A 1962 *Acta Cryst.* **15** 578
[11] Thomas J F 1968 *Phys. Rev.* **175** 955
[12] Vinet P, Ferrante J, Smith J R and Rose J H 1986 *J. Phys. C: Solid State Phys.* **19** L467
[13] Vinet P, Smith J R, Ferrante J and Rose J H 1987 *Phys. Rev.* B **35** 1945
[14] Syassen K and Holzapfel W B 1978 *J. Appl. Phys.* **49** 4427
[15] Dewaele A, Loubeyre P and Mezouar M 2004 *Phys. Rev.* B **70** 094112
[16] Hiki Y and Granato A V 1966 *Phys. Rev.* **144** 411
[17] Chantasiriwan S and Milstein F 1996 *Phys. Rev.* B **53** 14080
[18] Daw M S, Foiles S M and Baskes M I 1993 *Mater. Sci. Rep.* **9** 251
[19] Fluss M J, Smedskjaer L C, Chason M K, Legnini D G and Siegal R W 1978 *Phys. Rev.* B **17** 3444
[20] Dobson P S, Goodhew P J and Smallman R E 1967 *Phil. Mag.* **16** 9
[21] Murr L E 1975 *Interfacial Phenomena in Metals and Alloys* (Reading, MA: Addison-Wesley) p 145
[22] Stedman R and Nilsson G 1966 *Phys. Rev.* **145** 492
[23] Parrinello M and Rahman A 1982 *J. Chem. Phys.* **76** 2662
[24] Metropolis N, Rosenbluth A W, Rosenbluth M N, Teller A H and Teller E 1953 *J. Chem. Phys.* **21** 1087
[25] Chantasiriwan S and Milstein F 1998 *Phys. Rev.* B **58** 5996
[26] Ercolessi F and Adams J B 1994 *Europhys. Lett.* **26** 583

[27] Mishin Y, Farkas D, Mehl M J and Papaconstantopoulos D A 1999 *Phys. Rev.* B **59** 3393
[28] Giauque W F and Meads P F 1941 *J. Am. Chem. Soc.* **63** 1897
[29] Pochapsky T E 1953 *Acta Metall.* **1** 747
[30] Kamm G N and Alers G A 1964 *J. Appl. Phys.* **35** 327
[31] Gerlich D and Fisher E S 1969 *J. Phys. Chem. Solids* **30** 1197
[32] Perry F C 1970 *J. Appl. Phys.* **41** 1870
[33] Morris J R, Wang C Z, Ho K M and Chan C T 1994 *Phys. Rev.* B **49** 3109
[34] Lide D R (ed) 2007 *CRC Handbook of Chemistry and Physics* (Baco Raton, FL: CRC Press)
[35] Moriguchi K and Igarashi M 2006 *Phys. Rev.* B **74** 024111
[36] Brugger K 1964 *Phys. Rev.* **133** A1611